PNAS

Supporting Information for
Tailoring the Aluminum nanocrystal surface oxide for all-Aluminum-based antenna-reactor plasmonic photocatalysts

Aaron Bayles[1,5], Catherine J. Fabiano[7], Chuqiao Shi[3], Lin Yuan[1,5], Yigao Yuan[1,5], Nolan Craft[4], Christian R. Jacobson[1,5], Parmeet Dhindsa[1,5], Adebola Ogundare[1,5], Yelsin Mendez Camacho[3], Banghao Chen[7], Hossein Robatjazi[1], Yimo Han[3], Geoffrey F. Strouse[7], Peter Nordlander[4,5], Henry O. Everitt[1,2,4,5,6], and Naomi J. Halas[1,2,4,5]

Corresponding Author: Naomi J. Halas
Email: halas@rice.edu

This PDF file includes:

Figures S1 to S21
Supplementary Notes

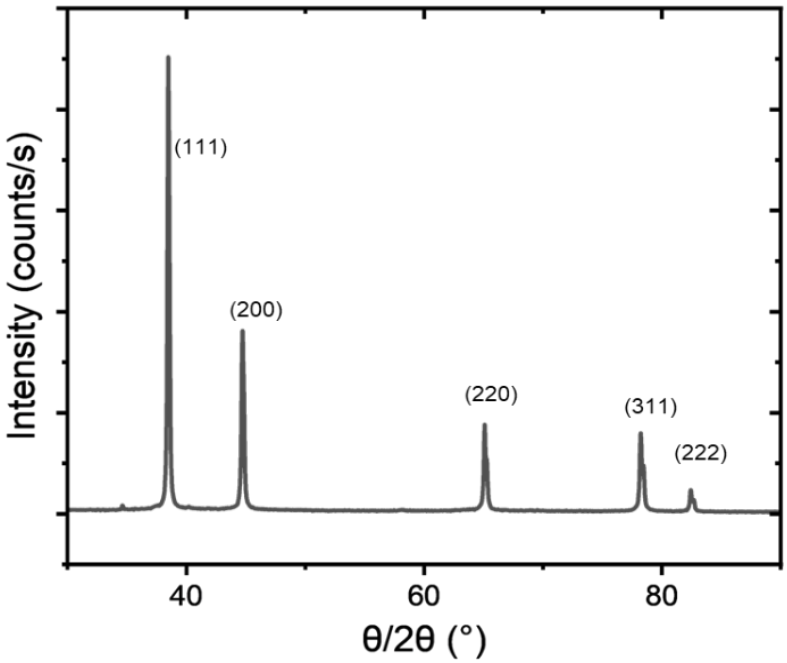

Fig. S1. XRD of untreated AlNCs. Only peaks pertaining to fcc aluminum are observed.

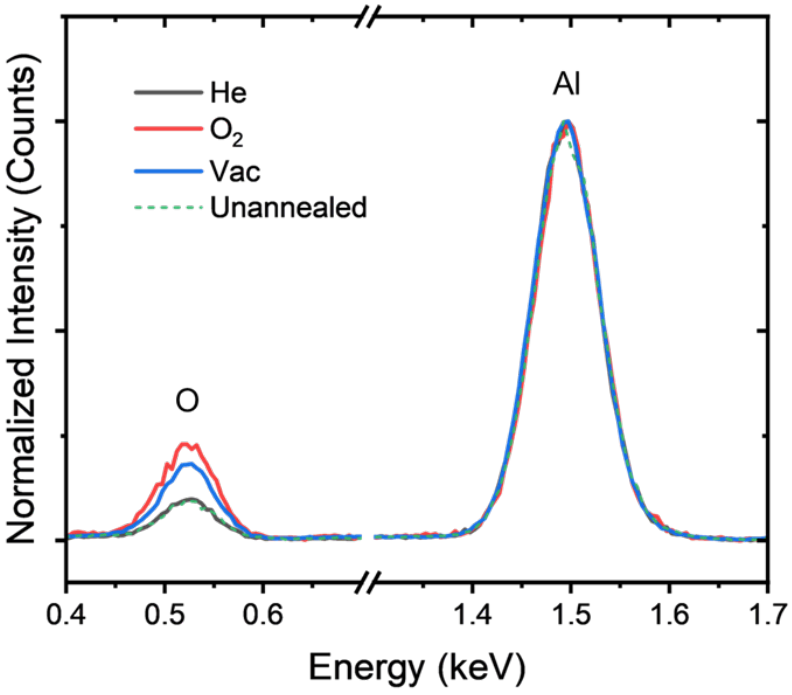

Fig. S2. Normalized EDX spectra of single unannealed and annealed AlNCs showing the relative signal of Al and O.

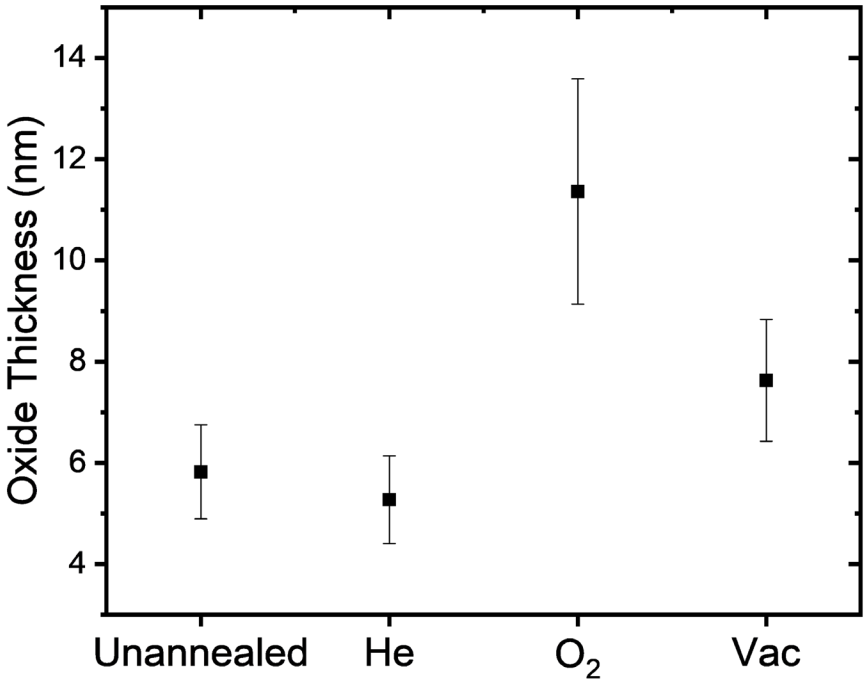

Fig S3. Oxide thickness measured in TEM as a function of annealing condition.

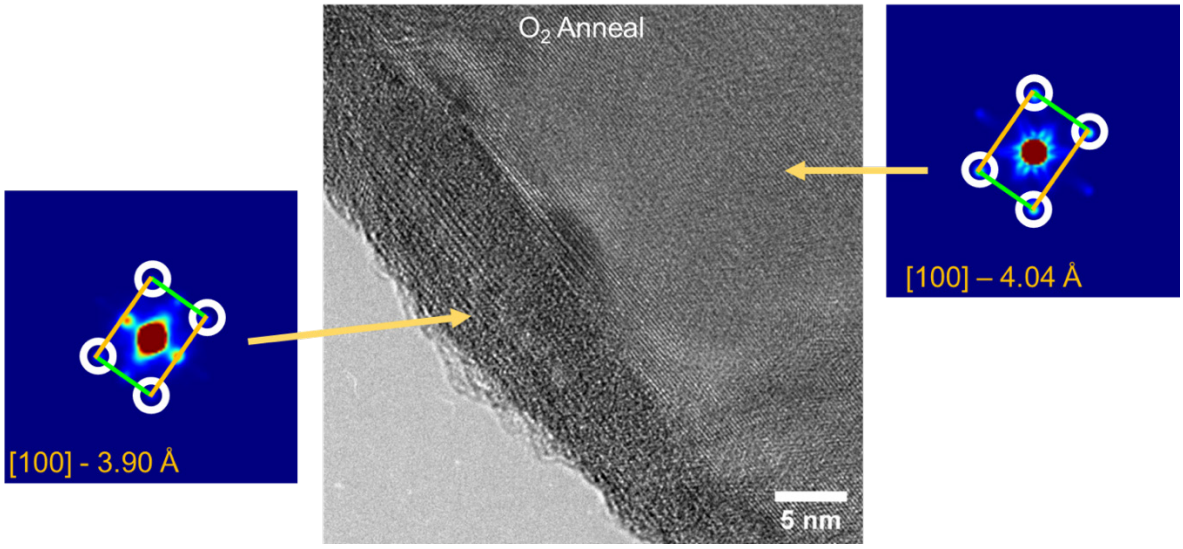

Fig S4. HRTEM image of the edge of an O_2-annealed AlNC, with FFT of the mean electron diffraction and measured lattice spacing for the core and shell regions.

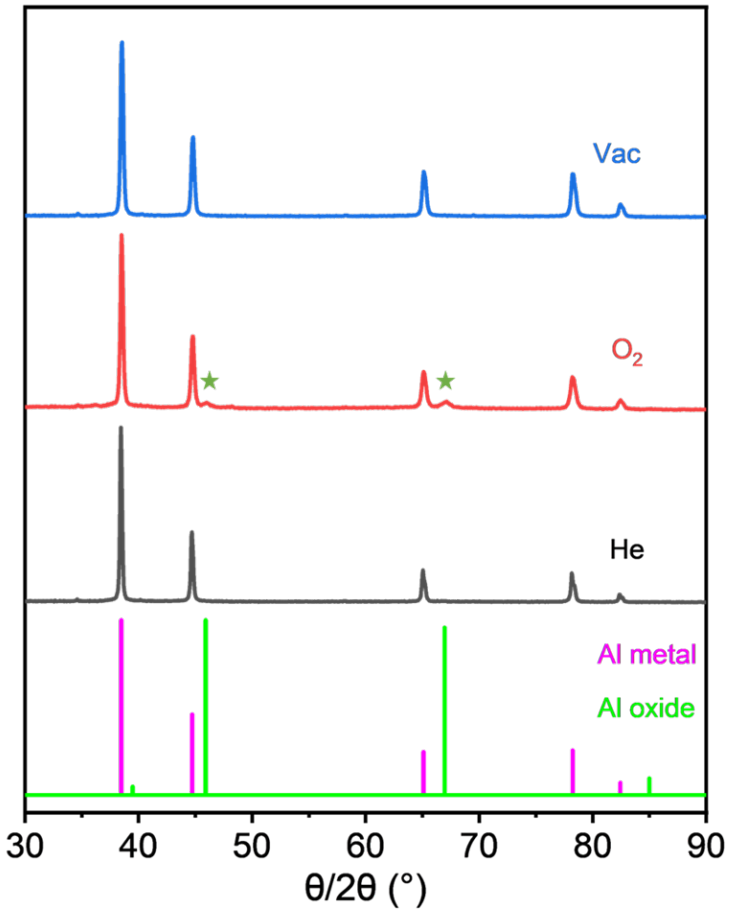

Fig S5. XRD patterns of annealed AlNCs compared to literature patterns. Oxide peaks in experimental diffractogram are marked with green stars.

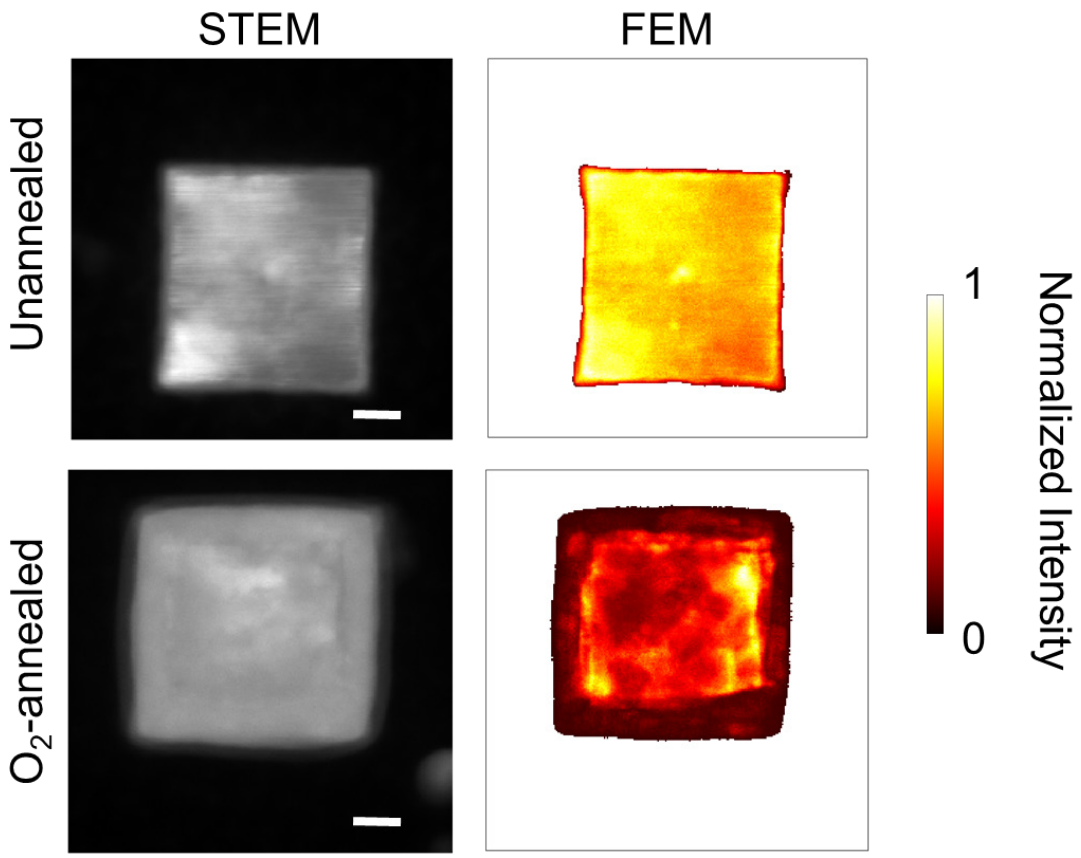

Fig S6. (Left column) STEM images of unannealed and O_2-annealed Al nanocubes. (Right column) Corresponding FEM maps of the images particles.

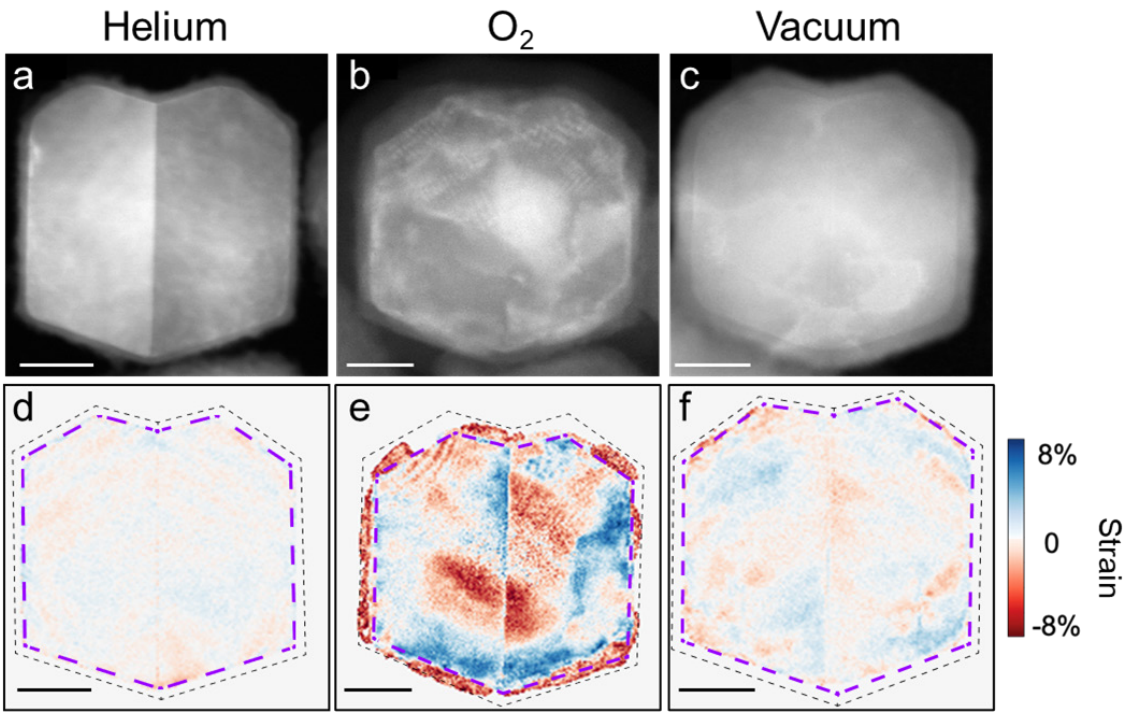

Fig S7. (a-c) HAADF-STEM images of single annealed AlNCs. Scale bars are 50 nm. (d-f) Corresponding 4D-STEM strain mapping. Black dashed outline shows total particle sizes, purple dashed outline shows metal-oxide interface.

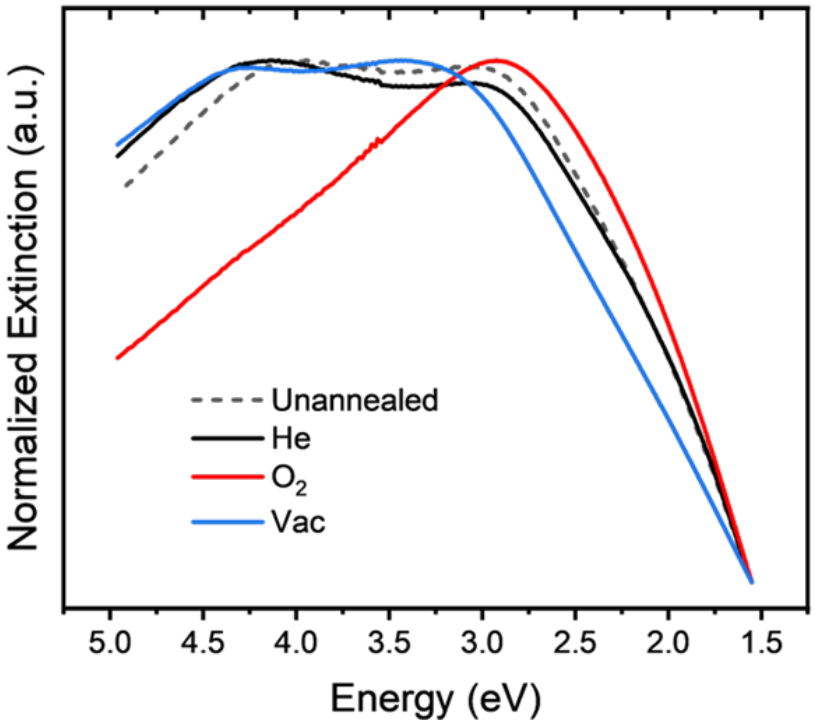

Fig S8. Experimental extinction spectra of unannealed and annealed AlNCs.

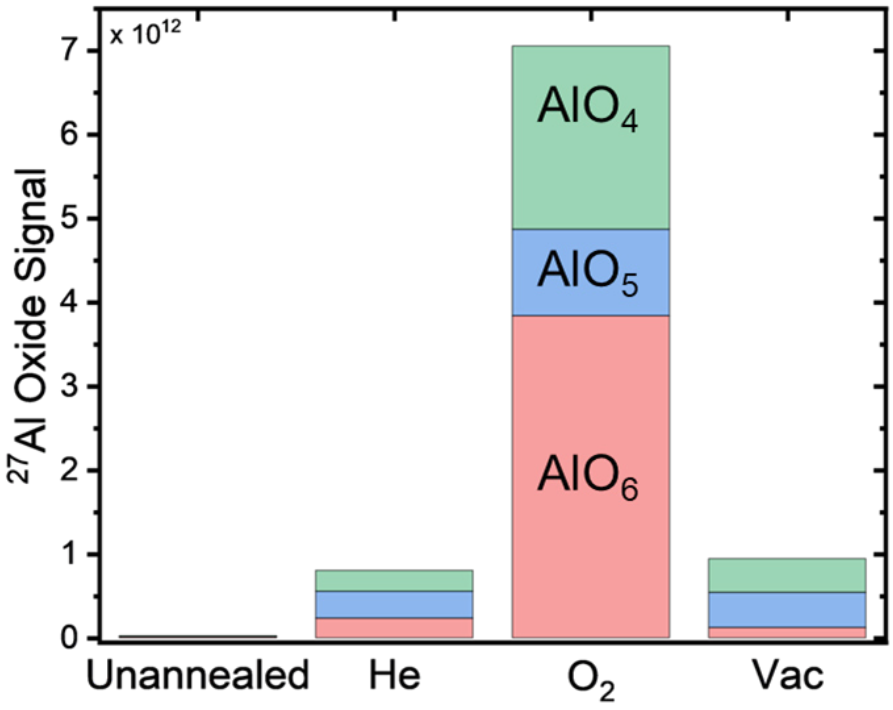

Fig S9: Absolute ^{27}Al ssNMR signal for each oxide coordination site in unannealed and annealed AlNCs.

	Site Coordination (%)		
Sample	AlO_4	AlO_5	AlO_6
Unannealed	23.48	31.17	45.35
He anneal	31.13	39.84	29.03
O_2 anneal	30.92	14.66	54.42
Vacuum anneal	42.46	33.59	12.95

Fig S3. Summary of ssNMR site coordination percentages.

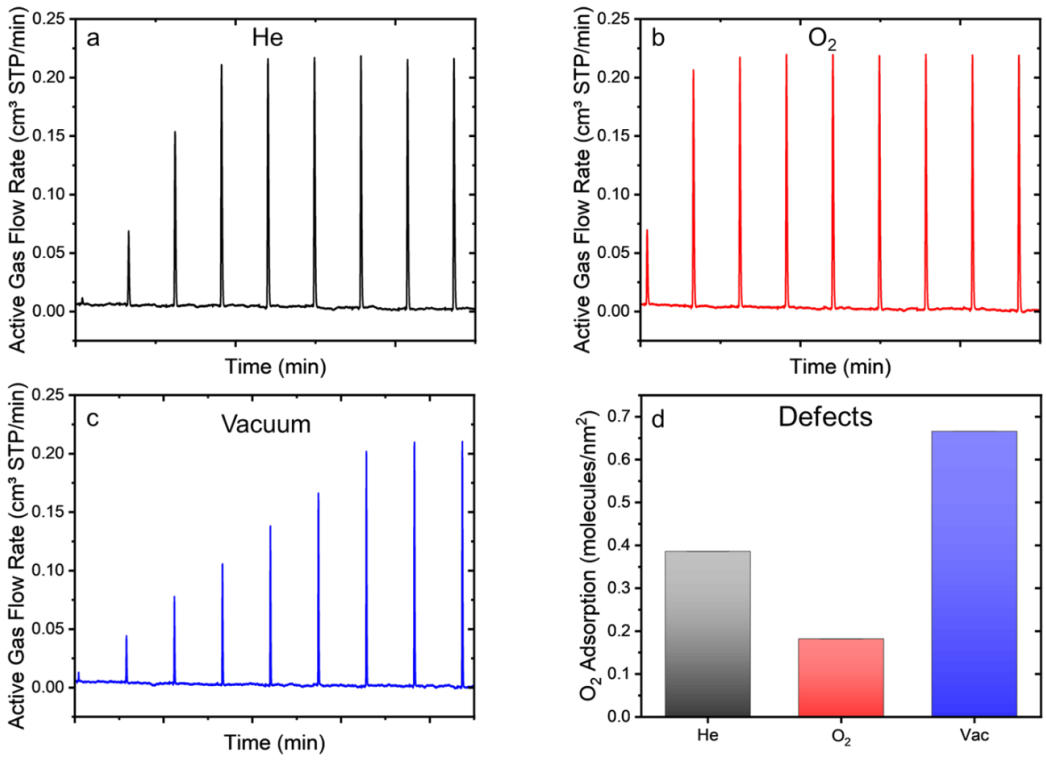

Fig S11. Cryogenic O_2 pulse chemisorption on annealed AlNCs. (a-c) Raw O_2 pulse data. Each peak corresponds to the injection of ~0.5mL of 10% O_2 in He into the gas flow over the annealed samples, after which only unadsorbed O_2 is detected by the thermal conductivity detector. (d) Surface defect density based on the amount of adsorbed O_2 calculated from the pulse chemisorption data.

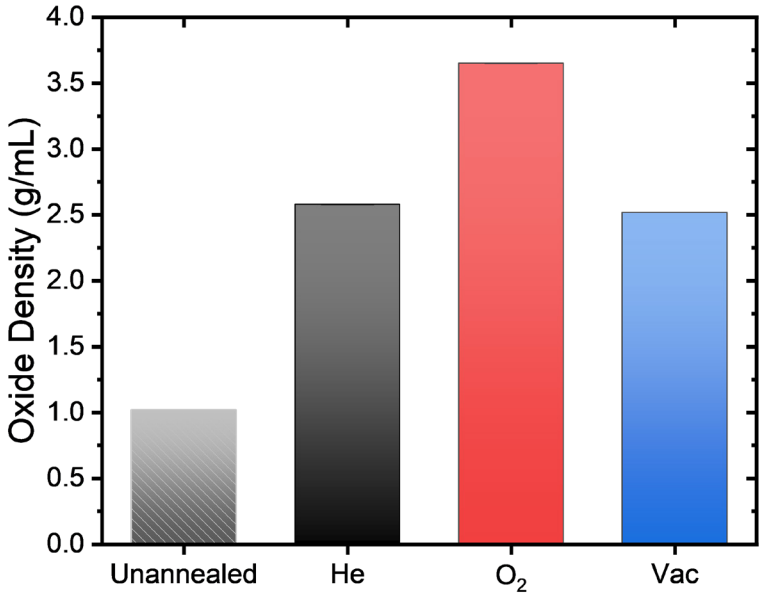

Fig S12. Oxide density of AlNCs.

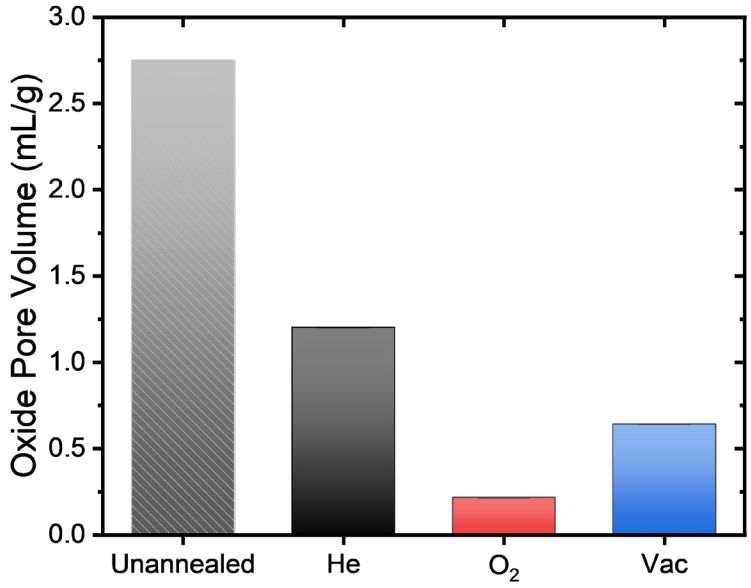

Fig S13. Oxide pore volume of annealed AlNCs.

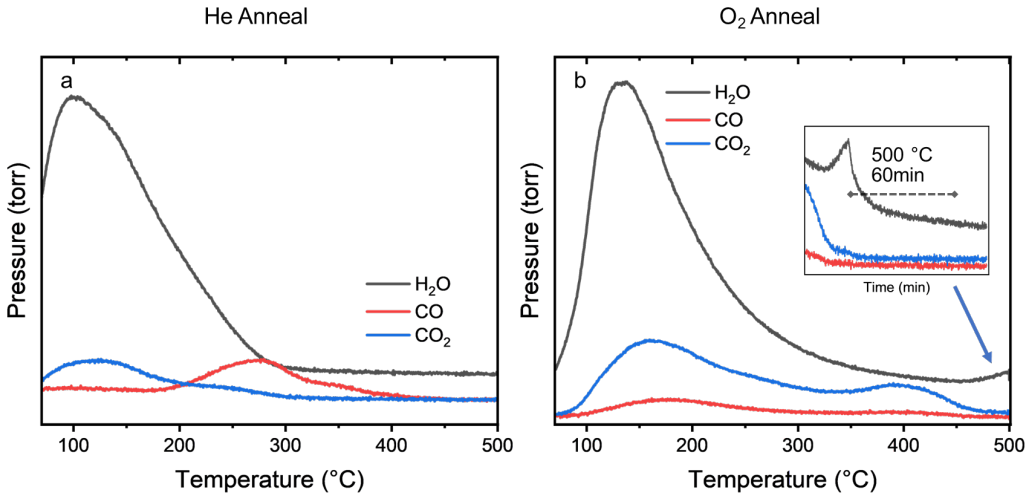

Fig S14. Mass spectrometer traces of outgassing during He (a) and O_2 (b) annealing. (b, inset) Time profile of gas desorption during O_2 annealing while temperature was held at 500 °C for one hour.

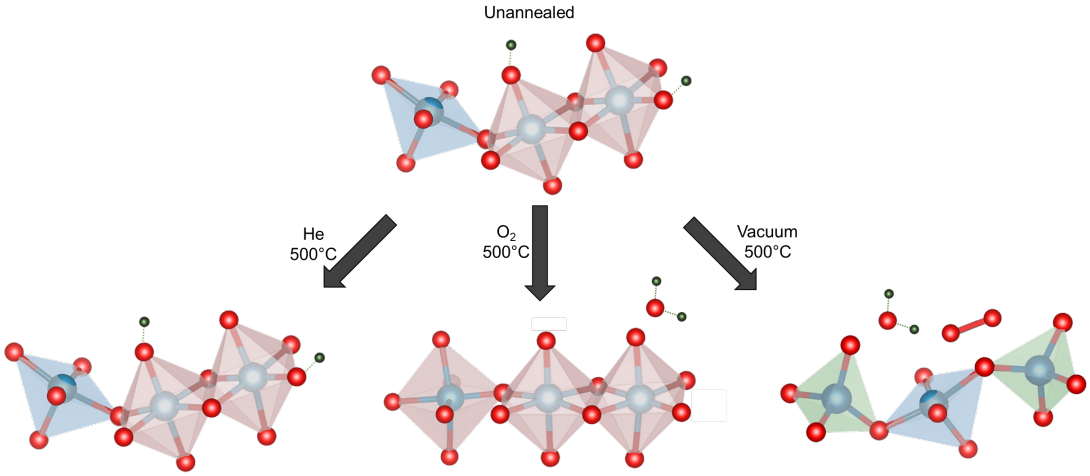

Fig S15. Graphical representation of the effect of annealing on the local alumina coordination and structure. He annealing causes no change except for the desorption of atmospheric H_2O and carbon contamination. O_2 annealing fills defect sites, increasing crystallinity, and oxidizes hydroxyl groups, which leave as H_2O. Vacuum annealing causes the conversion of AlO_6 to lower coordination sites through dehydration and dehydroxylation.

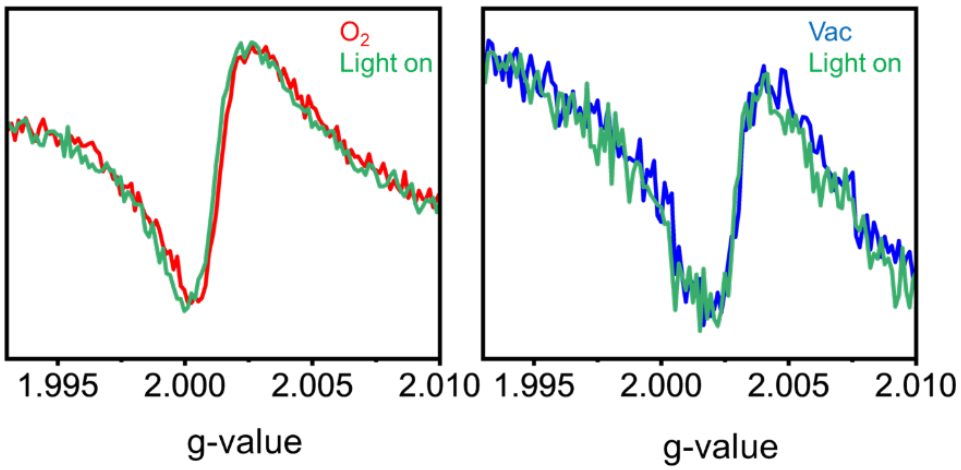

Fig S16. Comparison of illuminated and dark EPR signals for O_2-annealed (left) and Vacuum-annealed (right) AlNCs.

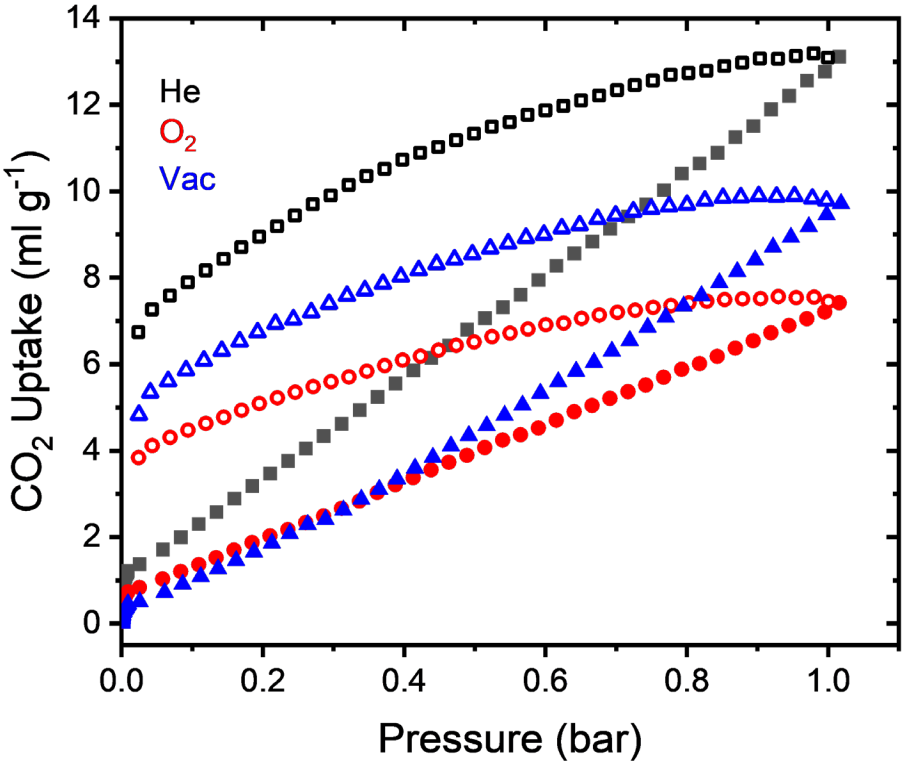

Fig S17. CO_2 uptake isotherms for the annealed AlNCs.

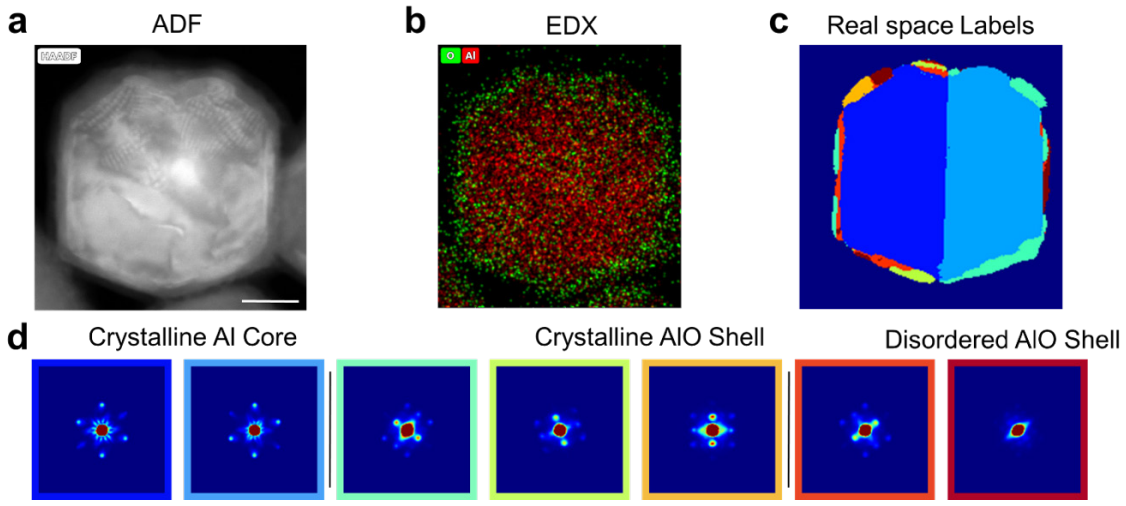

Fig S18. Unsupervised learning results on O_2-annealed AlNC 4D-STEM dataset. (a) Annular Dark Field image. (b) EDX. (c) Corresponding Real space labels of crystalline domains. (d) Mean cepstrum images for each domain cluster.

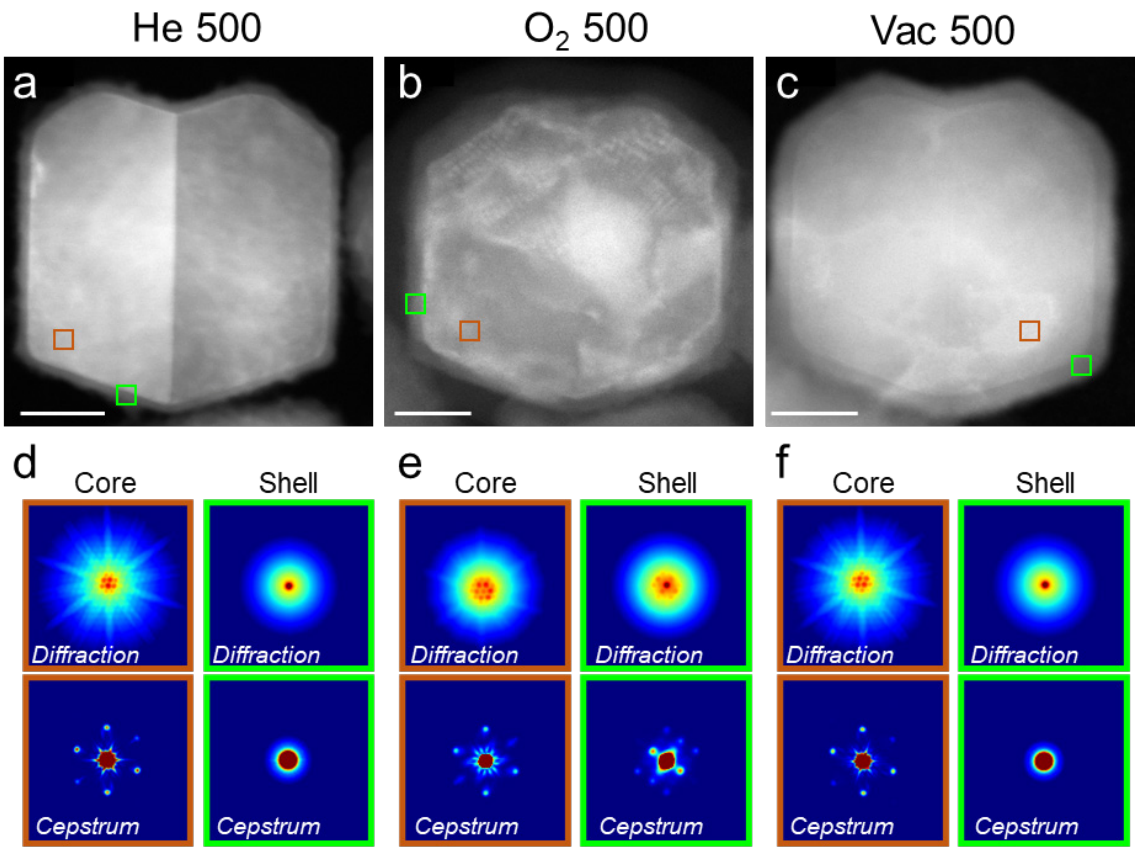

Fig S19. (a-c) HAADF-STEM images of single annealed AlNCs. Scale bars are 50 nm. (d-f) Mean electron diffraction and FFT of the diffraction (cepstrum) of core (orange) and oxide (green) region, noted with colored boxes.

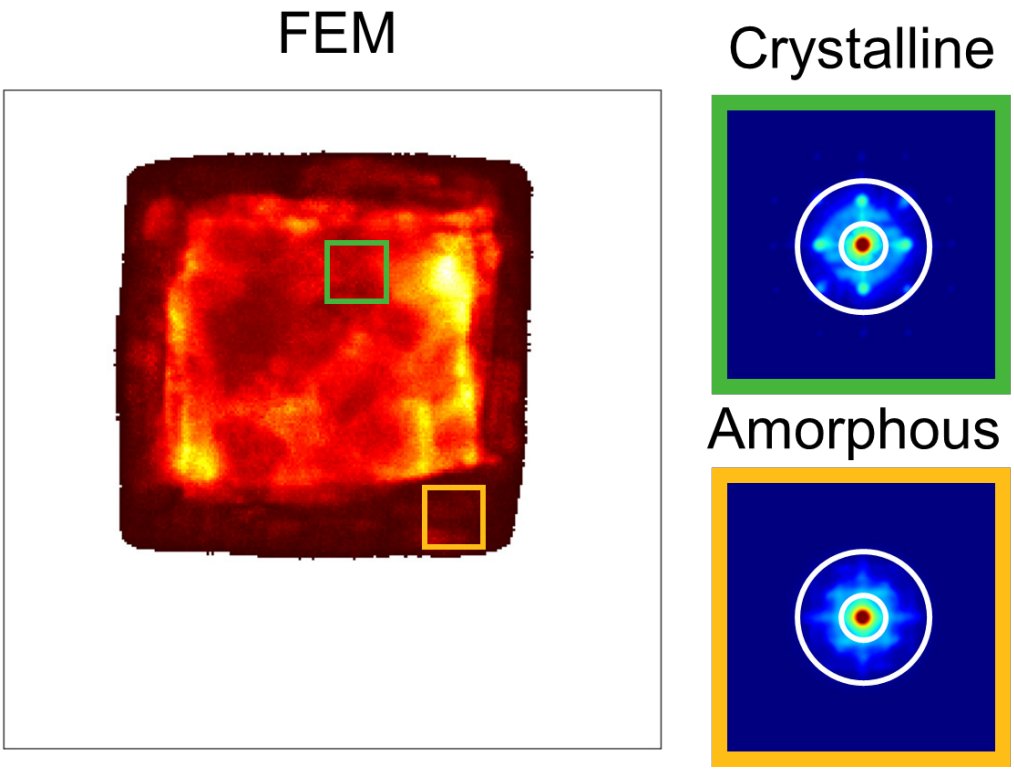

Fig S20. Processing of FEM image, demonstrating the difference between crystalline and amorphous areas. The middle range order regions are enclosed by the white rings

Supplementary Note 1

Oxide density was determined by first calculating the %mass of the oxide (μ_{oxide}) in each sample. By summing the integration of the metal and oxides peaks in ^{27}Al ssNMR, the total sample mass can be expressed by NMR signal intensity, and $\mu_{oxide} = \frac{\int 27Al\ Oxide\ Signal}{\int 27Al\ Total\ Signal}$. The oxide mass ($m_{oxide}$) can be expressed as $m_{oxide} = m_{sample} \times \mu_{oxide}$.

The volume of the oxide (V_{oxide}) can be calculated by modeling the nanoparticles as core-shell spheres where the volume of the shell is expressed by the equation $V_{oxide} = \frac{4}{3}\pi \times (r_{outer} - r_{core})$ where r is radius (Fig S. The outer and core radii are measured experimentally in TEM. Density (ρ) can then be calculated as $\rho = \frac{m_{oxide}}{V_{oxide}}$. However, a correction factor (C) must be introduced for two reasons: (1) Al metal and Al oxide may not produce the same ssNMR signal intensity as a function of mass and (2) volume is calculated for a single shell while the mass is calculated for a bulk sample. The correction factor is determined by using the γ-alumina of O_2-annealed as an internal density standard, as the density is known to be 3.6 g/mL[1]. The equation can then be rewritten as $\rho = \frac{m_{oxide}}{V_{oxide}} \times C$.

References:

1. Villars, P. γ-Al2O3 (Al2.67O4 m-γ cub) Crystal Structure: Datasheet from "PAULING FILE Multinaries Edition". (2022).